MITSUBISHI ELECTRIC RESEARCH LABORATORIES
http://www.merl.com

MPC for Coupled Station Keeping, Attitude Control, and Momentum Management of Low-Thrust Geostationary Satellites

Walsh, A.; Di Cairano, S.; Weiss, A.

TR2016-047 July 2016

Abstract

This paper develops a model predictive control (MPC) policy for simultaneous station keeping, attitude control, and momentum management of a nadir-pointing geostationary satellite equipped with three reaction wheels and four gimbaled electric thrusters that are located on the anti-nadir face of the satellite. The MPC policy works in combination with an innerloop SOp3q-based attitude controller that ensures the satellite maintains a nadir-pointing attitude. The MPC policy is able to maintain the satellite's position within a prescribed latitude and longitude window, while minimizing the v required by the thrusters. The MPC policy also enforces thruster pointing constraints and manages the satellite's stored momentum. With reference to simulation results, we explain how the MPC is tuned for station keeping, the need for an inner-loop attitude controller, and how these separate systems work together to achieve all the controller's objectives.

2016 American Control Conference (ACC)

MPC for Coupled Station Keeping, Attitude Control, and Momentum Management of Low-Thrust Geostationary Satellites

Alex Walsh*, Stefano Di Cairano† and Avishai Weiss‡

***Abstract*— This paper develops a model predictive control (MPC) policy for simultaneous station keeping, attitude control, and momentum management of a nadir-pointing geostationary satellite equipped with three reaction wheels and four gimbaled electric thrusters that are located on the anti-nadir face of the satellite. The MPC policy works in combination with an inner-loop $SO(3)$-based attitude controller that ensures the satellite maintains a nadir-pointing attitude. The MPC policy is able to maintain the satellite's position within a prescribed latitude and longitude window, while minimizing the Δv required by the thrusters. The MPC policy also enforces thruster pointing constraints and manages the satellite's stored momentum. With reference to simulation results, we explain how the MPC is tuned for station keeping, the need for an inner-loop attitude controller, and how these separate systems work together to achieve all the controller's objectives.**

I. Introduction

Recently, there has been significant interest in the utilization of low-thrust, high-specific-impulse electric engines for satellite control – both for propellant-efficient interplanetary trajectory design [1], [2], and for routine orbital station keeping [3]–[8]. Electric thrusters have considerably higher specific impulse than that of chemical thrusters, allowing for a reduction in propellant mass, thereby lowering launch costs and enabling larger payloads [9]. Conventional chemical thrusters produce hundreds of newtons for orbit control [10], and in geostationary Earth orbit (GEO), may be fired open-loop once every two weeks to compensate for satellite drift [11]. In contrast, the maximum thrust currently generated by state-of-the-art electric propulsion systems is in the hundreds of millinewtons [12], which for GEO, is on the order of the perturbation forces [13]. Thus, the utilization of electric thrusters poses new control challenges, requiring near continuous operation in order to provide the necessary imparted impulse, and suggest the use of closed-loop feedback control [3], [6], [7].

The problem of maintaining a low-thrust satellite in GEO is treated in [6], where the authors propose a model predictive control (MPC) policy for simultaneous station keeping and momentum management. The authors develop their control for a satellite equipped with three reaction wheels and six dual-axis thrusters mounted on each face of the satellite, enabling pure thrusts and torques applied in any direction and about any axis. In this paper, we expand on [6] to consider a realistic thruster configuration with gimbaled thrusters located on the satellite's anti-nadir face [3], [14], [15]. This arrangement leaves room on the satellite's other faces for antennas and solar panels, without the risk of thruster plume impingement.

However, the configuration also poses new challenges for control design, severely restricting the control action and making it more difficult to reject orbital perturbations. Furthermore, to both efficiently counteract the perturbation forces and allow for momentum unloading, the thrusters are permitted to gimbal. In doing so, they may also generate undesirable torques on the satellite, significantly coupling the satellite orbital and attitude dynamics. Thus, the need to treat concurrently both the "fast" attitude dynamics and the "slow" orbital dynamics present computational challenges in resource constrained hardware. With fast dynamics, a small discretization time-step is required. However, a long MPC prediction horizon is necessary for station keeping. A small discretization time step accompanied by a long prediction horizon results in a large and computationally challenging optimization problem.

The main contribution of this paper is the design of an inner-outer loop control architecture that overcomes the aforementioned challenges, where an outer-loop MPC policy operates in conjunction with an inner-loop $SO(3)$-based attitude controller for position, attitude, and momentum control. The paper begins with the description of the satellite model in Section II, followed by station-keeping MPC, model linearization, and constraints in Section III. The inner-loop attitude controller is introduced in Section IV. Closing remarks follow the main contribution in Section V.

The following notation will be used in all derivations. A frame of reference $\mathcal{F}_a$ is defined by a set of three orthonormal dextral basis vectors, and can be written as a vectrix $\underrightarrow{\boldsymbol{\mathcal{F}}}_a$, where $\underrightarrow{\boldsymbol{\mathcal{F}}}_a^{\mathsf{T}} = [\underrightarrow{a}^1 \;\; \underrightarrow{a}^2 \;\; \underrightarrow{a}^3]$. A physical vector describing the position of a point y_2 relative to point y_1 is written as $\underrightarrow{v}^{y_2 y_1}$. A physical vector can be resolved in any reference frame, such as, $\underrightarrow{v} = \underrightarrow{a}^1 v_{a_1} + \underrightarrow{a}^2 v_{a_2} + \underrightarrow{a}^3 v_{a_3} = [v_{a_1} \;\; v_{a_2} \;\; v_{a_3}]\underrightarrow{\boldsymbol{\mathcal{F}}}_a = \underrightarrow{\boldsymbol{\mathcal{F}}}_a^{\mathsf{T}} \mathbf{v}_a$, where the subscript a on the column matrix of components $\mathbf{v}_a$ indicates that the physical vector $\underrightarrow{v}$ is resolved in $\mathcal{F}_a$. Since $\underrightarrow{v} = \underrightarrow{\boldsymbol{\mathcal{F}}}_a^{\mathsf{T}} \mathbf{v}_a = \underrightarrow{\boldsymbol{\mathcal{F}}}_b^{\mathsf{T}} \mathbf{v}_b$, applying a left dot-product with $\underrightarrow{\boldsymbol{\mathcal{F}}}_b$ yields $\mathbf{v}_b = \underrightarrow{\boldsymbol{\mathcal{F}}}_b \cdot \underrightarrow{\boldsymbol{\mathcal{F}}}_a^{\mathsf{T}} \mathbf{v}_a = \mathbf{C}_{ba}\mathbf{v}_a$. The matrix $\mathbf{C}_{ba} \in SO(3)$ is a direction cosine matrix (DCM) defined by $\mathbf{C}_{ba} \triangleq \underrightarrow{\boldsymbol{\mathcal{F}}}_b \cdot \underrightarrow{\boldsymbol{\mathcal{F}}}_a^{\mathsf{T}}$, where $SO(3) = \{\mathbf{C} \in \mathbb{R}^{3\times 3} | \mathbf{C}^{\mathsf{T}}\mathbf{C} = \mathbf{1}, \det \mathbf{C} = 1\}$, and $\mathbf{1}$ is the identity matrix. Principal rotations about the $\underrightarrow{a}^i$ basis vector

*Ph.D. Candidate, Department of Aerospace Engineering, University of Michigan, Ann Arbor, MI 48109, USA. Email: aexwalsh@umich.edu

†Senior Principal Member Research Staff, Mitsubishi Electric Research Laboratories, Cambridge, MA 02139, USA. Email: dicairano@merl.com

‡Member Research Staff, Mitsubishi Electric Research Laboratories, Cambridge, MA 02139, USA. Email: weiss@merl.com

by an angle α are denoted by $\mathbf{C}_{ba} = \mathbf{C}_i(\alpha)$.

The "cross" operator maps a three-dimensional vector to a skew symmetric matrix, that is $(\cdot)^\times : \mathbb{R}^3 \to \mathfrak{so}(3)$, where $\mathfrak{so}(3) = \{\mathbf{U} \in \mathbb{R}^{3\times 3} | \mathbf{U} = -\mathbf{U}^\mathsf{T}\}$. The "uncross" map does the opposite where $(\cdot)^\vee : \mathfrak{so}(3) \to \mathbb{R}^3$, where $(\mathbf{v}^\times)^\vee = \mathbf{v}, \forall \mathbf{v} \in \mathbb{R}^3$. The skew-symmetric projection operator is $\mathcal{P}_a(\mathbf{U}) = \frac{1}{2}(\mathbf{U} - \mathbf{U}^\mathsf{T})$, for all $\mathbf{U} \in \mathbb{R}^{n\times n}$.

II. Satellite Model

Consider the satellite depicted in Fig. 1 that has three axisymmetric reaction wheels attached to a rigid bus in an orthogonal and mass balanced configuration. Four electric thrusters are located on the anti-nadir face of the satellite. The thrusters provide thrust in a line coincident with their position and the center of mass of the satellite, but are able to gimbal away from this nominal direction. The satellite's center of mass is denoted by c and has a bus-fixed frame $\mathcal{F}_p$. The frame $\mathcal{F}_g$ is the Earth Centred Inertial (ECI) frame, w is an unforced particle, and it is assumed that w is collocated with the center of the Earth. Each thruster has a frame $\mathcal{F}_i$, located at point t_i for thrusters $i = 1, \ldots, 4$.

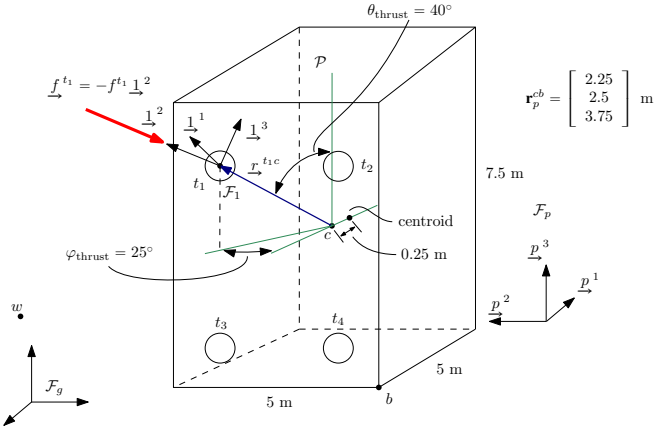

Fig. 1: Satellite $\mathcal{B}$ with platform $\mathcal{P}$ showing electric thrusters. A force $\underrightarrow{f}^{t_1}$ is shown when the thrust is perfectly in line with the center of mass of the satellite.

The equations of motion of the satellite are given by

$$\begin{aligned} \ddot{\mathbf{r}}_g^{cw} + \mu \frac{\mathbf{r}_g^{cw}}{\left\|\mathbf{r}_g^{cw}\right\|^3} &= \mathbf{a}_g^{\text{p}} + \frac{1}{m_{\mathcal{B}}} \mathbf{f}_g^{\text{thrust}}, \\ \mathbf{J}_p^{\mathcal{B}c} \dot{\boldsymbol{\omega}}_p^{pg} + \boldsymbol{\omega}_p^{pg^\times} \left(\mathbf{J}_p^{\mathcal{B}c} \boldsymbol{\omega}_p^{pg} + \mathbf{J}_s \dot{\boldsymbol{\gamma}}\right) + \mathbf{J}_s \boldsymbol{\eta} &= \boldsymbol{\tau}_p^{\text{p}} + \boldsymbol{\tau}_p^{\text{thrust}}, \\ \dot{\mathbf{C}}_{pg} &= -\boldsymbol{\omega}_p^{pg^\times} \mathbf{C}_{pg}, \\ \ddot{\boldsymbol{\gamma}} &= \boldsymbol{\eta}, \end{aligned} \tag{1}$$

where $\mathbf{r}_g^{cw}$ is the position of the satellite and $\boldsymbol{\gamma}$ is a column matrix containing the angle of rotation of each reaction wheel. The vector $\boldsymbol{\omega}_p^{pg}$ is the angular velocity of $\mathcal{F}_p$ relative to $\mathcal{F}_g$ resolved in $\mathcal{F}_p$. The matrix $\mathbf{J}_p^{\mathcal{B}c}$ is the moment of inertia of the satellite $\mathcal{B}$ relative to its center of mass, resolved in $\mathcal{F}_p$. Each thruster applies a force $\underrightarrow{f}^{t_i}$ at each point t_i, and is resolved in a frame dedicated to each thruster $\mathcal{F}_i$. The reaction wheel array has a moment of inertia $\mathbf{J}_s$ and the wheels are controlled with an acceleration $\boldsymbol{\eta}$. The term $\mathbf{a}_g^{\text{p}}$ represents the external perturbations on the satellite due to Earth's non spherical gravitational field, solar and lunar gravitational attraction, solar radiation pressure (SRP), and are defined in [6, Eq. (2)]. The term $\boldsymbol{\tau}_p^{\text{p}}$ represents the SRP perturbation torque, which assumes total absorption, and is given by [16, p. 229].

The thrusters are placed on the rear side of the satellite, and each thruster has a position $\underrightarrow{r}^{t_i b}$. The nominal thrust direction is along the vector $\underrightarrow{r}^{t_i c}$. The frame $\mathcal{F}_i$ has its $\underrightarrow{i}^2$ unit vector defined such that $\underrightarrow{i}^2 = \underrightarrow{r}^{t_i c} / |\underrightarrow{r}^{t_i c}|$. The DCM $\mathbf{C}_{ip}$ is defined using the geometry of the satellite. Each force $\underrightarrow{f}^{t_i}$ is applied at point t_i. The total force due to the thrusters applied to the satellite resolved in $\mathcal{F}_g$ is given by

$$\mathbf{f}_g^{\text{thrust}} = \sum_{i=1}^{4} \mathbf{f}_g^{t_i} = \mathbf{C}_{pg}^\mathsf{T} \sum_{i=1}^{4} \mathbf{C}_{ip}^\mathsf{T} \mathbf{f}_i^{t_i}. \tag{2}$$

The torque produced by the electric thrusters relative to the satellite's center of mass, resolved in the bus fixed frame $\mathcal{F}_p$ is given by

$$\boldsymbol{\tau}_p^{\text{thrust}} = \sum_{i=1}^{4} \mathbf{r}_p^{t_i c^\times} \mathbf{C}_{ip}^\mathsf{T} \mathbf{f}_i^{t_i}. \tag{3}$$

The gimbal angle of the thruster is a quantity that can be evaluated once the controller has found the control input $\mathbf{f}_i^{t_i}$. The gimbal angles comprise two angles, α_1 and α_3, which are depicted in Fig. 2. The angles are defined such that $\mathbf{f}_i^{t_i}$ can be described by two principal rotations, yielding

$$\mathbf{f}_i^{t_i} = -\mathbf{C}_3^\mathsf{T}(\alpha_3) \mathbf{C}_1^\mathsf{T}(\alpha_1) \mathbf{1}_2 \left\|\mathbf{f}_i^{t_i}\right\|. \tag{4}$$

The negative sign is due to the convention that at zero gimbal angle, the thrust is in the $-\underrightarrow{i}^2$ direction. The controller computes the thrust components resolved in $\mathcal{F}_i$, rather than a magnitude and two angles, because the latter produces a nonlinear problem and makes the optimization much more difficult.

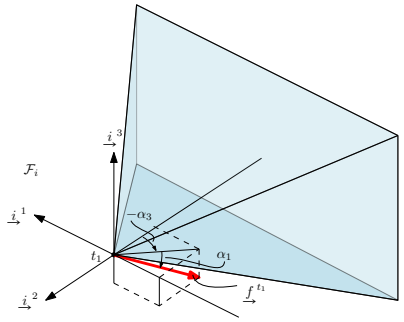

Fig. 2: A satellite thruster with gimbal angle and linear pointing constraint. In this figure, the force $\underrightarrow{f}^{t_i}$ does not satisfy the pointing constraint as it is outside the blue shaded pyramid.

III. MPC for Station Keeping, Momentum Management, and Attitude Control

The main contribution of this paper is the design of an architecture that allows for simultaneous station keeping, attitude control, and momentum management for the satellite shown in Fig. 1. The controller's objectives are to

1) maintain the satellite in the station keeping window,
2) minimize fuel consumption of the satellite,
3) ensure thrust remains within prescribed constraints,
4) maintain a nadir-pointing attitude, and
5) manage the reaction wheel speeds.

Following [6], an MPC policy is ideal for this task as it is naturally able to handle these objectives. The MPC controller solves a receding-horizon finite-time optimal control problem that is based on a system model subject to pointwise-in-time state and control constraints and a user-defined cost function. By using linearized equations of motion, linear equality and inequality constraints, and quadratic costs on the states and control, the MPC can be formulated as a quadratic programming (QP) problem. A QP can be solved quickly and efficiently, which makes it suited for satellites where on-board computing power may be limited.

A. Linearization for MPC

The dynamics (1) are resolved in Hill's frame $\mathcal{F}_h$ and linearized about a nominal circular orbit with mean motion n, angular velocity $\boldsymbol{\omega}_0$, in a nadir-pointing configuration defined by $\mathcal{F}_d$ with zero reaction wheel speed. The attitude error is parametrized by a $3-2-1$ Euler angle sequence given by $\mathbf{C}_{pd} = \mathbf{C}_{pg}\mathbf{C}_{dg}^{\mathsf{T}} = \mathbf{C}_1(\phi)\mathbf{C}_2(\theta)\mathbf{C}_3(\psi)$, where the angles ψ, θ and ϕ correspond to the yaw, pitch and roll of the satellite. The Euler angles are condensed to a column matrix $\delta\boldsymbol{\theta} \triangleq [\delta\phi \;\; \delta\theta \;\; \delta\psi]^{\mathsf{T}}$. Defining $\boldsymbol{\Omega} \triangleq \operatorname{diag}(-3n^2, 0, n^2)$, the linearized equations of motion are given by

$$\delta\ddot{\mathbf{r}} = -\boldsymbol{\Omega}\delta\mathbf{r} - 2\boldsymbol{\omega}_0^{\times}\delta\dot{\mathbf{r}} + \mathbf{a}_h^{\mathrm{p}} + \frac{1}{m_{\mathcal{B}}}\mathbf{C}_{dh}^{\mathsf{T}}\sum_{i=1}^{4}\mathbf{C}_{ip}^{\mathsf{T}}\mathbf{f}_i^{t_i} \tag{5a}$$

$$\delta\dot{\boldsymbol{\theta}} = -\boldsymbol{\omega}_0^{\times}\delta\boldsymbol{\theta} + \delta\boldsymbol{\omega} \tag{5b}$$

$$\begin{aligned}\delta\dot{\boldsymbol{\omega}} = &-\mathbf{J}_p^{\mathcal{B}c^{-1}}(\boldsymbol{\omega}_0^{\times}\mathbf{J}_p^{\mathcal{B}c} - (\mathbf{J}_p^{\mathcal{B}c}\boldsymbol{\omega}_0)^{\times})\delta\boldsymbol{\omega} \\ &- \mathbf{J}_p^{\mathcal{B}c^{-1}}\boldsymbol{\omega}_0^{\times}\mathbf{J}_s\delta\dot{\boldsymbol{\gamma}} - \mathbf{J}_p^{\mathcal{B}c^{-1}}\mathbf{J}_s\boldsymbol{\eta} + \sum_{i=1}^{4}\mathbf{r}_p^{t_ic^{\times}}\mathbf{C}_{ip}^{\mathsf{T}}\mathbf{f}_i^{t_i}.\end{aligned} \tag{5c}$$

The discrete-time linear model with time step Δt is

$$\mathbf{x}_{k+1} = \mathbf{A}\mathbf{x}_k + \mathbf{B}_{w,d}\mathbf{w}_k + \mathbf{B}\mathbf{u}_k, \tag{6}$$

where $\mathbf{w}_k$ models the disturbances $\mathbf{a}_h^{\mathrm{p}}$. Equation (6) is used along a prediction horizon $k = 1, \ldots, N$. During the prediction horizon, we can approximate the disturbances $\mathbf{w}_k, k = 1, \ldots, N$ as the disturbances associated with the satellite at its desired position, since the satellite will always be kept very close to the desired position during correct operation. The control input $\mathbf{u}_k$ is $\mathbf{u}_k = [\mathbf{f}_1^{t_1^{\mathsf{T}}} \;\; \ldots \;\; \mathbf{f}_4^{t_4^{\mathsf{T}}} \;\; \boldsymbol{\eta}^{\mathsf{T}}]^{\mathsf{T}}$.

B. Constraints

The linearized dynamics are resolved in $\mathcal{F}_h$, with $\delta\mathbf{r} = [r_1 \;\; r_2 \;\; r_3]^{\mathsf{T}}$. As such, the station keeping constraints are given by $|\delta r_2| \leqslant r_0\tan(\lambda_{1,\max})$, $|\delta r_3| \leqslant r_0\tan(\lambda_{2,\max})$, where $\lambda_{1,\max}$ and $\lambda_{2,\max}$ are the maximum tolerable longitude and latitude errors, respectively, and where r_0 is the nominal orbital radius.

The thrust pointing constraint is enforced by constraining the thrust to remain in the interior of four planes, and is described by the element-wise constraints

$$\mathbf{D}_i\mathbf{f}_i^{t_i} \geqslant \mathbf{0}, \tag{7}$$

where each of the four rows of $\mathbf{D}_i$ contains a normal vector describing a plane. The four planes in (7) are visualized in Fig. 2. The thrust magnitude constraint is a norm constraint $\left\|\mathbf{f}_i^{t_i}\right\| \leqslant f_{\max}$, which is nonlinear. This can be approximated as linear by imposing the constraint $\left|\mathbf{f}_i^{t_i}\right| \leqslant \mathbf{f}_{\max}$, where $\mathbf{f}_{\max} = [1 \;\; 1 \;\; 1]^{\mathsf{T}} f_{\max}$, and $f_{\max}$ is the maximum allowable thrust. Note that while this approximation works well in our case, several other approximations of the norm are possible.

The attitude error of the satellite is also subject to the element-wise constraint $|\delta\boldsymbol{\theta}| \leqslant \boldsymbol{\theta}_{\max}$, where $\boldsymbol{\theta}_{\max}$ is the maximum allowable attitude error.

C. MPC for Station Keeping With Attitude Control

The MPC policy solves the finite-horizon optimal control problem at time t

$$\min_{\mathcal{U}_t} \mathbf{x}_{N|t}^{\mathsf{T}}\mathbf{P}\mathbf{x}_{N|t} + \sum_{k=0}^{N-1}\mathbf{x}_{k|t}^{\mathsf{T}}\mathbf{Q}\mathbf{x}_{k|t} + \mathbf{u}_{k|t}^{\mathsf{T}}\mathbf{R}\mathbf{u}_{k|t}, \tag{8}$$

subject to

$$\begin{aligned}&\mathbf{x}_{k+1|t} = \mathbf{A}\mathbf{x}_{k|t} + \mathbf{B}_{w,d}\mathbf{w}_{k|t} + \mathbf{B}\mathbf{u}_{k|t}, k = 0, \ldots, N-1, \\ &\mathbf{x}_{0|t} = \mathbf{x}(t), \quad \left|\delta r_{2_{k|t}}\right| \leqslant r_0\tan(\lambda_{1,\max}), \\ &\left|\delta\boldsymbol{\theta}_{k|t}\right| \leqslant \boldsymbol{\theta}_{\max}, \quad \left|\delta r_{3_{k|t}}\right| \leqslant r_0\tan(\lambda_{2,\max}), \\ &\mathbf{D}_i\mathbf{f}_{i_{k|t}}^{t_i} \geqslant \mathbf{0}, \quad \left|\mathbf{f}_{i_{k|t}}^{t_i}\right| \leqslant \mathbf{f}_{\max}, \;\; i = 1, \ldots, 4,\end{aligned}$$

where N is the prediction horizon, $\mathcal{U}_t = \{\mathbf{u}_{0|t}, \ldots, \mathbf{u}_{N-1|t}\}$, and $\mathcal{U}_t^* = \{\mathbf{u}_{0|t}^*, \ldots, \mathbf{u}_{N-1|t}^*\}$ is the optimizer of (8). The matrices $\mathbf{Q} \succcurlyeq 0$ and $\mathbf{R} > 0$ are state and control weights, and $\mathbf{P} > 0$ is the terminal cost determined from the solution of the Discrete Algebraic Riccati Equation (DARE) for the infinite horizon problem. The control is selected as $\mathbf{u}(t) = \mathbf{u}_{0|t}^*$.

Since the terminal cost $\mathbf{P}$ is a solution of the DARE, local stability of the equilibrium is guaranteed. Near equilibria, if state and control constraints are inactive, the solution of (8) is equivalent to that of an LQR. Feasibility of (8) is guaranteed by relaxing the state constraints to soft constraints with the introduction of slack variables.

D. Simulation Results

The purpose of the first simulation is to produce results similar to [6], demonstrating that MPC applied to the nonlinear dynamics (1) is able satisfy control objectives 1-5. The satellite's mass is $m_{\mathcal{B}} = 4000$ kg. The mean surface area is $S = 200$ m^2, surface reflectance $c_{\text{refl}} = 0.6$, and the solar facing area is $S_{\text{facing}} = 37.5$ m^2. Each reaction wheel has a mass $m_{\mathcal{W}_k} = 20$ kg, a radius $r_{\mathcal{W}_k} = 0.75$ m, and a height of $\ell_{\mathcal{W}_k} = 0.2$ m. For simplicity, the three reaction wheels are assumed to coincide with the satellite's center of mass. Earth's gravitational parameter is $\mu_{\mathrm{E}} = 398600$ km^3/s^2, the Sun's is $\mu_{\mathrm{S}} = 132712440018$ km^3/s^2, the Moon's is $\mu_{\mathrm{M}} = 4902.8$ km^3/s^2. Earth's J_2 parameter is $J_2 = 1.081874\cdot10^{-3}$,

its radius is $R_{\text{E}} = 6378$ km, and the solar radiation pressure constant is $C_{\text{srp}} = 4.5 \cdot 10^{-6}$ N/m^2.

The simulation time is set to 90 minutes with $\Delta t = 5$ minutes. The satellite must remain in a station keeping window of $\pm 0.01^\circ$ in latitude and longitude. The maximum thrust is $f_{\max} = 0.1$ N, with a pointing angle $\alpha_1 = \alpha_3 = 36^\circ$. The maximum allowable error on the Euler angles is $\pm 0.02^\circ$. The weighting matrices for the states in the simulation are $\mathbf{Q}_{\mathbf{r}} = \mathbf{Q}_{\dot{\mathbf{r}}} = \mathbf{1} \cdot 10^{-3}$, $\mathbf{Q}_{\boldsymbol{\theta}} = \mathbf{1} \cdot 10^{4}$, $\mathbf{Q}_{\boldsymbol{\omega}} = \mathbf{1} \cdot 10^{2}$, and $\mathbf{Q}_{\dot{\boldsymbol{\gamma}}} = \mathbf{1} \cdot 10^{5}$. The initial condition is set on January 1, 2000 with a semimajor axis of 42164.2 km and all other orbital elements zero. The attitude initial conditions are $\mathbf{C}_{pg} = \mathbf{C}_3(180^\circ)$, $\boldsymbol{\omega}_p^{pg} = \boldsymbol{\omega}_0$, and $\dot{\boldsymbol{\gamma}}(0) = [50 \;\; 50 \;\; 50]^{\mathsf{T}}$ rad/s, which corresponds to $\mathbf{C}_{pd} = \mathbf{1}$ and $\boldsymbol{\omega}_p^{pd} = \mathbf{0}$.

The results are shown in Fig. 3. As in [6], the MPC policy is able to drive the reaction wheel speed to zero (Fig. 3a). However, the optimal control $\mathbf{u}_k$ causes the pointing constraint to be violated, and this is due to several reasons. First, the dynamics of the nonlinear system and the linear system diverge with nonzero reaction wheel speeds. For example, when the reaction wheel speeds increase from 0 to 50 rad/s, a lightly damped mode appears at 0.5 rad/s, and a higher damped mode appears at 95.3 rad/s. Since there is a large difference between the linearized and nonlinear systems, the MPC policy predicts that the attitude constraints are satisfied when the linear dynamics are propagated forward in time, as shown by the dot-dashed line in Fig. 3b. However, when the control is applied to the nonlinear system, the constraints are in fact violated. Second, in [6], the thrusters are able to create pure torques that are decoupled from body forces. With the thruster configuration in this paper, a thruster torque simultaneously creates a net body force. This effect couples the orbital and attitude dynamics, which complicates control.

This simulation identifies additional key problems with an MPC control policy that handles both attitude control and station keeping. For attitude control in [6], $\Delta t = 10$ min, and here $\Delta t = 5$ min are used to handle the relatively "fast" attitude dynamics. Station keeping dynamics are much slower than the attitude dynamics, and thus the discretization of the orbital dynamics do not require small time steps. To take advantage of the station keeping dynamics, a horizon of at least half an orbit is needed. A small time step ($\Delta t = 5$ min) coupled with a large prediction horizon (15 h) dramatically increases the size of the optimization problem ($N = 180$). Moreover, this optimization would need to be solved every 5 minutes instead of every hour, which would require a considerable increased use of onboard resources.

IV. MPC with Inner-Loop Attitude Control

To overcome the problems discussed in the previous section, an inner-loop attitude controller is proposed, with control architecture described in Fig. 4. The inner-loop controls the attitude via the reaction wheels, while the MPC policy controls the closed-loop satellite/attitude controller system. Therefore, the linearization of the open-loop system (5) is no longer adequate, and the MPC requires the closed-loop satellite/attitude controller to be linearized.

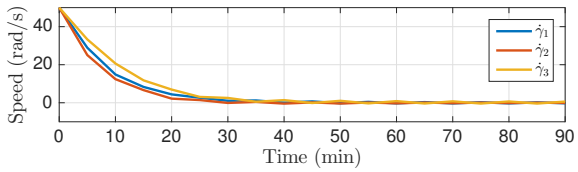

(a) Reaction wheel speeds decreasing from 50 rad/s.

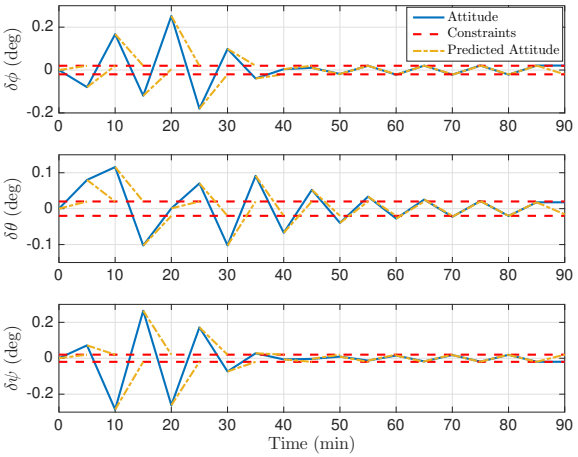

(b) Attitude error (in solid blue), attitude constraints (in dashed red), and predicted attitude from linearization (in dot-dashed yellow).

Fig. 3: Simulation for MPC controller without inner-loop control and $\Delta t = 5$ min.

A non-adaptive form of the controller proposed in [17] is used for the inner-loop attitude controller as it provides almost global asymptotic stability for attitude tracking and is capable of harmonic disturbance rejection. For an explanation of "almost global", see [17]. With respect to the attitude controller, the SRP torque and the torques due to the electric thrusters are considered to be attitude disturbances.

It is assumed that the torque disturbance is the output of an LTI system $\mathbf{A}_d, \mathbf{C}_d$. Defining $\mathbf{S} \triangleq -\mathcal{P}_a(\mathbf{C}_{pd})^\vee$, we obtain $\dot{\mathbf{S}} = \mathcal{P}_a(\boldsymbol{\omega}_p^{pd^\times}\mathbf{C}_{pd})^\vee$, and $\boldsymbol{\omega}_p^{pd} = \boldsymbol{\omega}_p^{pg} - \mathbf{C}_{pd}\boldsymbol{\omega}_d^{dg}$. The disturbance $\boldsymbol{\tau}_p^{\text{p}}$ is estimated by

$$\dot{\hat{\mathbf{d}}} = \mathbf{A}_d\hat{\mathbf{d}} + \mathbf{B}_d(\boldsymbol{\omega}_p^{pd} + \mathbf{K}_1\mathbf{S}), \tag{9a}$$

$$\hat{\boldsymbol{\tau}}_{\text{dist}} = \mathbf{C}_d\hat{\mathbf{d}}, \tag{9b}$$

where $\mathbf{K}_1 = \mathbf{K}_1^{\mathsf{T}} > 0$ is a gain and where $\mathbf{B}_d$ is designed such that (9) is positive real. Next define

$$\begin{aligned}
\boldsymbol{\nu}_1 &\triangleq \boldsymbol{\omega}_p^{pg^\times}(\mathbf{J}_p^{\mathcal{B}_c}\boldsymbol{\omega}_p^{pg} + \boldsymbol{J}_s\dot{\boldsymbol{\gamma}}) - \mathbf{J}_p^{\mathcal{B}_c}(\mathbf{K}_1\dot{\mathbf{S}} + \boldsymbol{\omega}_p^{pd^\times}\boldsymbol{\omega}_p^{pg}),\\
\boldsymbol{\nu}_2 &\triangleq -\hat{\boldsymbol{\tau}}_{\text{dist}},\\
\boldsymbol{\nu}_3 &\triangleq -\mathbf{K}_v(\boldsymbol{\omega}_p^{pd} + \mathbf{K}_1\mathbf{S}) - \mathbf{K}_p\mathbf{S},
\end{aligned} \tag{10}$$

where $\mathbf{K}_v = \mathbf{K}_v^{\mathsf{T}} > 0$ and $\mathbf{K}_p = \mathbf{K}_p^{\mathsf{T}} > 0$. The attitude control law is given by

$$\boldsymbol{\eta} = -\mathbf{J}_s^{-1}(\boldsymbol{\nu}_1 + \boldsymbol{\nu}_2 + \boldsymbol{\nu}_3). \tag{11}$$

Substituting the linearization of (11) into (5c) yields

$$\delta\dot{\boldsymbol{\omega}} = \boldsymbol{\tau}_p^{\text{thrust}} + [-\mathbf{K}_1 + \boldsymbol{\omega}_0^\times - \mathbf{J}_p^{\mathcal{B}c^{-1}}\mathbf{K}_v]\delta\boldsymbol{\omega} - \mathbf{J}_p^{\mathcal{B}c^{-1}}\mathbf{C}_d\hat{\mathbf{d}} + \Big[\mathbf{K}_1\boldsymbol{\omega}_0^\times - \boldsymbol{\omega}_0^\times\boldsymbol{\omega}_0^\times + \mathbf{J}_p^{\mathcal{B}c^{-1}}(\mathbf{K}_v\boldsymbol{\omega}_0^\times - \mathbf{K}_v\mathbf{K}_1 - \mathbf{K}_p)\Big]\delta\boldsymbol{\theta}, \quad (12)$$

where the SRP torque disturbance has been ignored. The term $\mathbf{C}_d\hat{\mathbf{d}}$ is the output of (10), and so the linearization of (9) is also required, and is given by

$$\dot{\hat{\mathbf{d}}} = \mathbf{A}_d\hat{\mathbf{d}} + \mathbf{B}_d\delta\boldsymbol{\omega} + \mathbf{B}_d(\mathbf{K}_1 - \boldsymbol{\omega}_0^\times)\delta\boldsymbol{\theta}, \quad (13a)$$

$$\hat{\boldsymbol{\tau}}_{\text{dist}} = \mathbf{C}_d\hat{\mathbf{d}}. \quad (13b)$$

The linearized prediction model for MPC is based on (5a), (5b), (12), (13), with states $\mathbf{x} = [\delta\mathbf{r}^\mathsf{T} \;\; \delta\dot{\mathbf{r}}^\mathsf{T} \;\; \delta\boldsymbol{\theta}^\mathsf{T} \;\; \delta\boldsymbol{\omega}^\mathsf{T} \;\; \delta\dot{\boldsymbol{\gamma}}^\mathsf{T} \;\; \hat{\mathbf{d}}^\mathsf{T}]^\mathsf{T}$. The change to the MPC policy (8) is that while the regulation of reaction wheel speeds $\dot{\boldsymbol{\gamma}}$ is still an objective, their acceleration $\boldsymbol{\eta}$ is no longer a control input determined as part of the optimization, but is now prescribed by the inner-loop control (11). This ensures that the MPC operates by controlling the thrusters in a way that causes the attitude controller (11) to reduce the reaction wheel speeds, and is possible because the MPC policy uses a closed-loop attitude model that captures the action of the attitude controller.

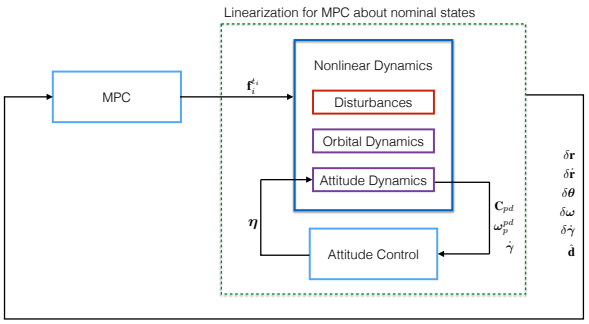

Fig. 4: MPC with inner-loop controller.

A. Simulation Results

The simulation with the inner-loop controller has almost all the same parameters as in Section III-D. The weighting matrices of these simulations are $\mathbf{Q}_\mathbf{r} = \text{diag}(0, 1, 1)$, $\mathbf{Q}_{\dot{\mathbf{r}}} = \mathbf{0}$ and $\mathbf{R} = \mathbf{1} \cdot 10^4$ to ensure that control is heavily penalized. The state weight is placed on longitude and latitude deviations. It is possible to use minimal weighting on the states because the station keeping constraints are built into the MPC policy. The weighting for the attitude related states are $\mathbf{Q}_{\boldsymbol{\theta}} = \mathbf{Q}_{\boldsymbol{\omega}} = \mathbf{1} \cdot 10^{-3}$, $\mathbf{Q}_{\dot{\boldsymbol{\gamma}}} = \mathbf{1} \cdot 10^{-2}$, and $\mathbf{Q}_{\hat{\mathbf{d}}} = \mathbf{0}$. The matrix $\mathbf{B}_d$ is determined by choosing $\mathbf{Q}_d = \mathbf{1} \cdot 0.05$, solving $\mathbf{A}_d^\mathsf{T}\mathbf{P}_d + \mathbf{P}_d\mathbf{A}_d = -\mathbf{Q}_d$ for $\mathbf{P}_d$, and then setting $\mathbf{B}_d = \mathbf{C}_d^\mathsf{T}\mathbf{P}_d^{-1}$. The horizon for MPC is chosen to be 15 hours to exploit the periodicity of the orbital disturbances. In addition, the dynamics are discretized using $\Delta t = 1$ h, as in [6], which is now possible because the fast attitude dynamics are managed by the inner-loop controller, and thus $N = 15$. The initial conditions are the same as Section III-D, except with $\dot{\boldsymbol{\gamma}} = \mathbf{0}$. The simulation is run for 425 orbits, but only the last year (365 orbits) is used for analysis to isolate the steady state of the system (see Fig. 5).

Fig. 5a shows that the satellite remains within the station keeping window. Fig. 5c shows the attitude error, which remains within 0.02°. Fig. 5d shows that the reaction wheel speed is controlled and does not increase without bound, as is the case in simulations where momentum management is not performed. Fig. 5b shows the cumulative Δv produced by each thruster, and the Δv due to the net force of the thrusters, resolved in $\mathcal{F}_h$. The Δv_3 is slightly less than 60 m/s, which is expected due to the out-of-plane perturbations. The total $\Delta v = 100.97$ m/s is 22.3 m/s more than required for station keeping only. The extra thrust is needed to counteract the solar radiation pressure torque and to manage the momentum of the reaction wheels.

Fig. 6 shows the last five orbits are plotted for enhanced detail. The reaction wheel speeds are cyclic over an orbit as expected. The thrusters are held constant over a one hour period, and the MPC solution results in only two thrusters being active at a time, as shown in Fig. 6d. Either the two North thrusters (forces at t_1 and t_2), or the two South thrusters (forces at t_3 and t_4) are active simultaneously. Note that due to the nature of the MPC policy, the thrust is held constant for one hour, and thus the gimbal angles are also constant. Gimbal angles do not change from $+36^\circ$ to -36° from one hour to the next, but do so in increments. The gimbal angles are often at their limits, which indicates that the thrusters are almost always creating some sort of torque, and implying that the reaction wheels are always in use.

V. Closing Remarks

Autonomous closed-loop feedback control for station keeping operations will increase the safety, robustness, and reliability of satellites. In this paper, we presented an MPC policy with an inner-loop $SO(3)$-based attitude controller that is able to satisfy station keeping constraints, while also providing momentum management. The $SO(3)$-based attitude controller is also able to keep the satellite's attitude error within the pointing constraints. All this can be achieved for a satellite configuration with the thrusters located on the anti-nadir face of the satellite, which is convenient for satellite design but challenging for control.

References

[1] J. A. Starek and I. V. Kolmanovsky, "Nonlinear model predictive control strategy for low thrust spacecraft missions," *Optimal Control Applications and Methods*, vol. 35, no. 1, pp. 1–20, 2014.

[2] O. Abdelkhalik and E. Taheri, "Approximate on-off low-thrust space trajectories using fourier series," *Journal of Spacecraft and Rockets*, vol. 49, no. 5, pp. 962–965, 2012.

[3] D. Losa, M. Lovera, J.-P. Marmorat, T. Dargent, and J. Amalric, "Station keeping of geostationary satellites with on-off electric thrusters," in *Proc. 2006 IEEE International Conference on Control Applications*, pp. 2890–2895, 2006.

[4] A. Sukhanov and A. Prado, "On one approach to the optimization of low-thrust station keeping manoeuvres," *Advances in Space Research*, vol. 50, no. 11, pp. 1478 – 1488, 2012.

[5] Y. Ulybyshev, "Long-term station keeping of space station in lunar halo orbits," *Journal of Guidance, Control, and Dynamics*, vol. 38, no. 6, pp. 1063–1070, 2014.

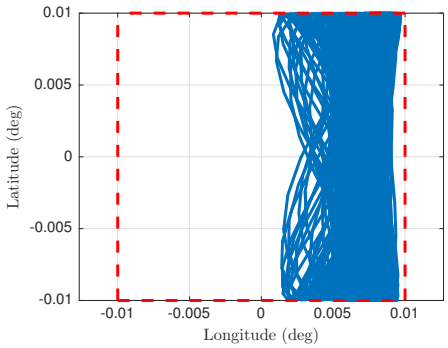

(a) Latitude and longitude error.

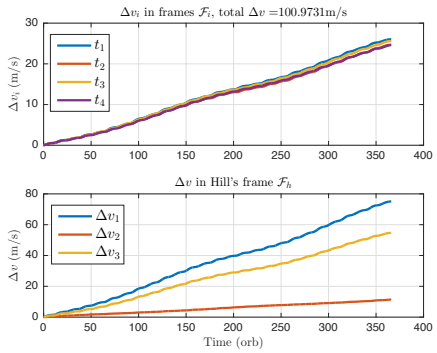

(b) Δv from each thruster and net Δv resolved in $\mathcal{F}_h$.

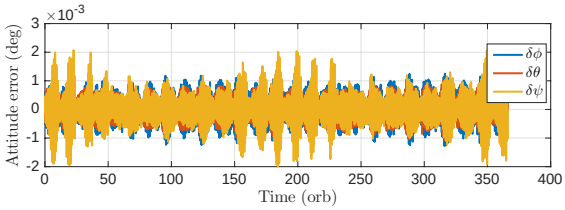

(c) Euler angle attitude error.

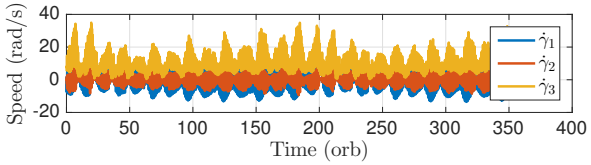

(d) Reaction wheel speeds.

Fig. 5: One year simulation for MPC controller with inner-loop control

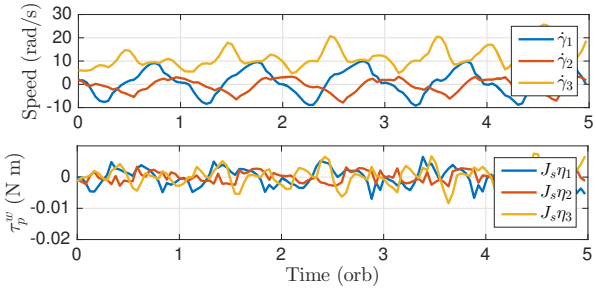

(a) Reaction wheel speeds and input.

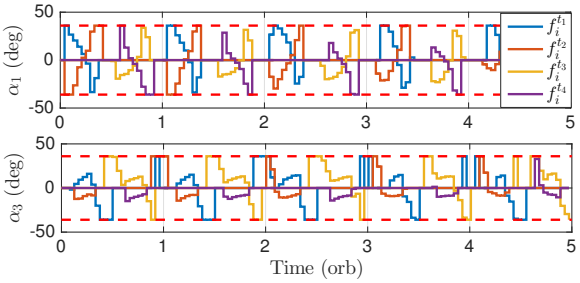

(b) Gimbal angles for each thruster with 36° constraint.

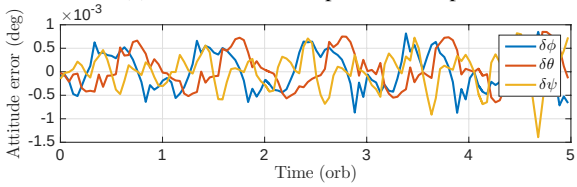

(c) Attitude error. Maximum error is 0.02°.

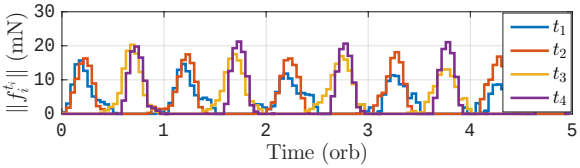

(d) Thrust magnitude. Maximum thrust is 100 mN.

Fig. 6: Close-up of 5 orbits detailing reaction wheels and thrusters.

[6] A. Weiss, U. Kalabic, and S. Di Cairano, "Model predictive control for simultaneous station keeping and momentum management of low-thrust satellites," in *Proc. 2015 American Control Conference*, pp. 2305–2310, 2015.

[7] U. Kalabic, A. Weiss, S. Di Cairano, and I. Kolmanovsky, "Station-keeping and momentum-management on halo orbits around L2: Linear-quadratic feedback and model predictive control approaches," in *25th AAS/AIAA Space Flight Mechanics Meeting, AAS 15-307*, 2015.

[8] A. Garulli, A. Giannitrapani, M. Leomanni, and F. Scortecci, "Autonomous low-earth-orbit station-keeping with electric propulsion," *Journal of Guidance, Control, and Dynamics*, vol. 34, no. 6, pp. 1683–1693, 2011.

[9] M. Martinez-Sanchez and J. E. Pollard, "Spacecraft electric propulsion – an overview," *Journal of Propulsion and Power*, vol. 14, no. 5, pp. 688–699, 1998.

[10] J. R. Wertz and W. J. Larson, eds., *Spacecraft Mission Analysis and Design*. Microcosm Press, 3rd ed., 1999.

[11] E. M. Soop, *Handbook of Geostationary Orbits*. Springer, 1994.

[12] D. Herman, G. C. Soulas, J. L. Van Noord, and M. J. Patterson, "NASA's evolutionary xenon thruster (NEXT) long-duration test results," *Journal of Propulsion and Power*, vol. 28, pp. 625–635, 2015/09/22 2012.

[13] R. R. Bate, D. D. Mueller, and J. E. White, *Fundamentals of Astrodynamics*. Dover Publications Inc., 1971.

[14] J. Climer, "Boeing: World's first all-electric propulsion satellite begins operations," Internet: http://boeing.mediaroom.com/index.php?s=20295&item=129516, 10 Sept. 2015, [22 Sept. 2015].

[15] B. M. Anzel, "Method and apparatus for a satellite station keeping." U.S. Patent 5 443 231, August 22, 1995.

[16] A. H. J. de Ruiter, C. J. Damaren, and J. R. Forbes, *Spacecraft Dynamics and Control: An Introduction*. Chichester, West Sussex, U.K.: John Wiley & Sons, Ltd, 2013.

[17] A. Weiss, I. Kolmanovsky, D. S. Bernstein, and A. Sanyal, "Inertia-free spacecraft attitude control using reaction wheels," *Journal of Guidance, Control, and Dynamics*, vol. 36, no. 5, pp. 1425–1439, 2013.